Elastoplasticity in dissipative heavy-ion collisions

M. Rhein,[1,*] R. Barth,[1] E. Ditzel,[1] H. Feldmeier,[2] E. Kankeleit,[1] V. Lips,[1] C. Müntz,[1] W. Nörenberg,[1,2] H. Oeschler,[1] A. Piechaczek,[1] W. Polai,[1] and I. Schall[1]

[1] *Institut für Kernphysik, Technische Hochschule, D-64289 Darmstadt, Germany*

[2] *Gesellschaft für Schwerionenforschung, D-64220 Darmstadt, Germany*

(Received 19 July 1993)

The spectral distributions of δ electrons emitted in dissipative heavy-ion collisions represent an established tool to study the time evolution of the collision process. Especially, the yield of high-energy δ electrons, which are measured for the first time up to an energy of 8 MeV, reflects short time scales and offers a unique possibility to examine the short deceleration phase at the beginning of the collision, which takes place within a few 10^{-22} s. The δ-electron spectra measured in dissipative collisions of Pb+Pb at an incident energy of 12 MeV/nucleon are compared with theoretical predictions using a coupled-channels formalism. The nuclear trajectories needed as input for the calculations are obtained from reaction models. Using nuclear trajectories calculated within the one-body dissipation model give a far too low yield of high-energy δ electrons indicating that the deceleration predicted by this model is too slow. The new dissipative diabatic model, which takes into account a non-Markovian dissipation at the beginning of the collision and which ascribes elastoplastic properties to nuclear matter, is able to reproduce both the fast deceleration and the long nuclear contact time deduced from the experimental data.

PACS number(s): 25.70.Lm

I. INTRODUCTION AND SUMMARY

Measurements of mass, charge, and momentum distributions of the final products, obtained in a heavy-ion reaction, yield only indirect information on the time evolution of the collision. It is very difficult to "see"—in the sense of receiving signals from a luminous source—the dynamical development of the nuclear system, because all signals emitted during the collision are blurred by the subsequent "glowing" of the excited nuclei. For example, in deeply inelastic collisions the promptly emitted neutrons may give information on nonequilibrium excitations and, due to diffraction effects in the mean field, also to a certain extent on the nuclear shape. The analysis is, however, rather model dependent and it is difficult to separate these neutrons from those emitted statistically by the excited fragments.

Another kind of "light" emitted by the nuclear source are γ rays. The measured γ spectrum constitutes a flash of photons created mainly by individual proton-neutron collisions. An exception are the γ quanta from the giant dipole resonance of a hot compound nucleus which allows an estimate of the deformation of the nuclear shape [1]. This is "light" from an equilibrated system. The information on the dynamical evolution during the initial phase of the collision is contained in photons created coherently by the collective nuclear charge current. Estimates [2] have shown that the cross section is much too low to separate the coherent from the statistical γ rays.

In this work we investigate "light" which comes from the atomic electron cloud around the colliding nuclei. The time dependence of the charge distribution of the nuclear system is felt most by the electrons in the innermost shells. In about 1 out of 100 lead-on-lead collisions a δ electron is propelled from the K shell into the continuum. Its energy spectrum is solely determined by the time dependence of the Coulomb potential. A great advantage of the δ-electron spectroscopy is the fact that the emission mechanism is theoretically well understood [3] in terms of atomic coupled-channel calculations. Of course there is also a nuclear contribution which is carefully corrected. As is shown in Sec. III B the background of conversion electrons, which is deduced from the simultaneously measured γ spectrum, is about a factor of 5–50 lower than the δ-electron yield depending on the collision selected. This is another important advantage compared to the type of γ spectroscopy mentioned above.

The aim of this paper is to investigate the time evolution of the nuclear shape degrees of freedom (the most characteristic one is the internuclear distance, hence we study trajectories) in ^{208}Pb on ^{208}Pb collisions by the method of δ-electron spectroscopy [3,4].

For electron energies up to 4 MeV the dependence of the spectral distribution of electrons and positrons on the nuclear trajectories is well documented in various publications [5–9] and is thus only briefly reviewed here. Throughout the paper, atomic coupled-channels calculations [10] are used, but the basic idea is best illustrated by the scaling model [4]. In this approach the transition amplitude a_{if} for the emission of a bound electron, is given by the Fourier transform of the quantity $\dot{R}(t)/R(t)$ by

$$a_{if} \propto \frac{1}{E_{if}} \int_{-\infty}^{\infty} dt \frac{\dot{R}(t)}{R(t)} \exp\left(i \frac{E_{if}}{\hbar} t\right), \qquad (1)$$

*Present address: Argonne National Laboratory, Physics Bldg. 203, Argonne, IL 60439.

where E_{if} is the difference between the initial and final energy of the electron. The quantity $R(t)$ denotes twice the time-dependent root-mean-square (rms) radius of the charge distribution of the two nuclei and is equivalent to the center-to-center distance for large R values [11]. Equation (1) shows that the information on the trajectory is essentially summarized in the ratio $\dot{R}(t)/R(t)$. The reason is that the K-shell electron, due to the broad spatial distribution of its wave function, feels only the angle average of the Coulomb potential. The spectral shapes calculated within the scaling model are in good agreement with the more elaborate coupled-channels calculations [10] which are used in the following analysis.

For the theoretical description of heavy-ion collisions several reaction models have been developed during the past two decades which reproduce a large body of nuclear data. The history of these developments and the knowledge reached is well reviewed in various textbooks on nuclear physics [12–14] and they are not discussed here.

The δ-electron spectra are mainly determined by two features of the trajectories. One is a time delay compared to Coulomb trajectories which is caused by the interplay of conservative and frictional forces when the nuclei are in contact. Typical contact times of $t_{\rm int} \approx 10^{-21}$ s lead to a depletion in the δ-electron spectra at an energy around 2–3 MeV. Due to statistical fluctuations in $t_{\rm int}$ for a given impact parameter [15] and the experimental limitation in selecting narrow impact-parameter regimes from the experimental data the minimum is washed out. It remains, however, a steeper decrease of the spectra for electron energies below 2 MeV [5–9]. By this observation, a model-independent evidence was found for the connection of dissipative reactions with a time delay. In the reaction models [15–17] that are able to describe the observed prolonged contact times, the time delay is essentially due to the development of a pronounced neck during the outgoing part of the trajectory, as discussed, e.g., in Ref. [9].

The other feature of dissipative heavy-ion collisions is the fast deceleration of the nuclei at the beginning of the collision, which leads to a rapid change of $\dot{R}/R(t)$ and thus to the emission of high-energy δ electrons [18–20]. The deceleration takes place within a few 10^{-22} s, a time scale that can only be investigated by measuring the spectral distribution of δ electrons up to high energy. The maximal energy measured in the present work is 8 MeV which corresponds to a time resolution of 5×10^{-22} s.

As an example for the predicted time scale of the deceleration, Fig. 1 shows the two-center distance between the nuclei as a function of time as predicted by three different reaction models for central collisions of Pb+Pb at 12 MeV/nucleon incident energy. Although the time evolution is quite different, the finally dissipated energy is about equal and does not reflect the dissimilarities in the trajectories. In the framework of phenomenological reaction models [15,16] the friction coefficients are adjusted to experimental nuclear reaction data. As an example the phenomenological trajectory model of Schmidt, Toneev, and Wolschin [16], in which the nuclei are treated as nonoverlapping ellipsoids, is used. Figure 1 shows that

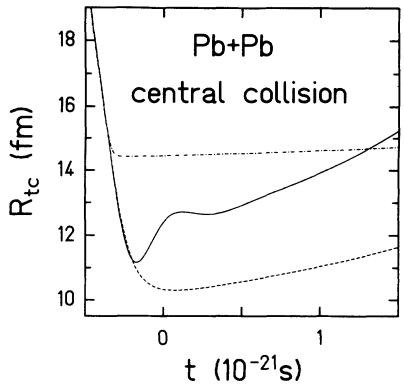

FIG. 1. Time evolution of the two-center distance for central collisions of Pb+Pb at 12 MeV/nucleon incident energy (solid line: dissipative diabatic model [19,20], dashed line: one-body dissipation model [17], dashed-dotted line: phenomenological model [16]).

this model leads to a fast stopping when the nuclei touch (dash-dotted line), much faster than the deceleration predicted by the one-body dissipation model [17] (dashed line). Here the deceleration is mainly due to friction forces which are calculated microscopically, based on the ideas of the wall and window dissipation [21].

For short time scales, since the deceleration takes place within a few 10^{-22} s, the Markov assumption applied to these models is questionable since the memory time is of the same order of magnitude. Therefore, a consistent description of the deceleration phase has to be taken into account memory effects. Essential memory effects in the dissipation process have been treated within the diabatic approach to dissipative collective motion and shown to cause an elastoplastic behavior in nuclear dynamics [22]. In the analysis of the δ-electron spectra we take advantage of the close relationship of dissipative diabatic dynamics to the one-body dissipation approach. By replacing the Markovian friction force (local in time) in the one-body dissipation model by an elastoplastic force (nonlocal in time) according to Ref. [22], we define a dissipative diabatic (elastoplastic) model as will be explained in Sec. IV A. The trajectory obtained with the new dissipative diabatic model is depicted as a solid line in Fig. 1. It exhibits a fast stopping followed by an oscillation. The discussion in Sec. IV C will show that this elastoplastic behavior is responsible for the enhanced yield of high-energetic δ electrons.

In order to obtain sufficient yield in the high-energy part of the δ-electron spectra we performed an experiment using the collision system ^{208}Pb+^{208}Pb at an incident energy of 12 MeV/nucleon which corresponds to 6.3 MeV/nucleon above the Coulomb barrier. The large relative velocity of the nuclei is needed to get a substantial deceleration when the nuclear forces set in. Electrons were detected up to an energy of 8 MeV to obtain information down to very short time scales.

In summary, in the study of ^{208}Pb+^{208}Pb collisions at 12 MeV/nucleon a very fast radial deceleration has been deduced from the yield of the high-energetic part of the δ-electron spectra. The stopping in the radial motion is much stronger than predicted by the one-body dissi-

pation model [17]. The new dissipative diabatic model not only allows to account in a consistent way for the two aspects of the experimental data, the long contact times and the fast stopping, but also for the correlations between scattering angles and total kinetic-energy loss. This model implies that the fast deceleration is followed by a giant vibration of the combined A=416 system. The successful description of the data strongly supports the existence of an elastoplastic behavior of nuclear matter in dissipative heavy-ion collisions.

II. EXPERIMENTAL SETUP

The experiment was carried out with the TORI spectrometer [23], installed at the UNILAC accelerator of GSI, Darmstadt. About 10^9 ions of ^{209}Pb per second impinged on ^{12}C-backed ^{208}Pb targets of $\approx$350 μg/cm^2 thickness. The TORI spectrometer is a magnetic transport system designed to measure simultaneously electrons and positrons in coincidence with the scattered heavy ions. A schematic view of the apparatus is depicted in Fig. 2. On one side of the target the apparatus is considered as an S-shaped solenoid. Electrons and positrons produced at the target position are transported to different detector systems by spiraling along the field lines. Due to field gradient in the S-shaped field, electrons and positrons experience a drift in opposite directions and they are separated in space after having passed the first quarter turn of the torus. Here electrons are detected by an array of three alcohol-cooled Si(Li) counters. Two detectors with an active area of 1.44 cm^2 and 5 mm depletion depth were positioned to detect preferentially electrons with energies up to 2.5 MeV. The third detector with an area of 3 cm^2 and 8 mm depletion depth was placed to detect electrons with energies between 1 and 3.5 MeV. In this way, a pileup of the more frequent low-energy electrons is avoided. Electrons which do not hit a detector are stopped by a Beryllium-plated, semicircular diaphragm.

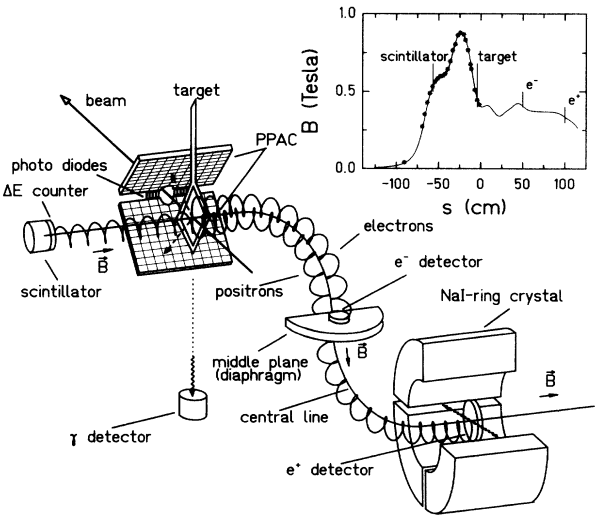

FIG. 2. Schematic view of the TORI spectrometer and its detector components. The insert shows the magnetic field strength along the middle line. The symbols denote measured points; the positions of the various detectors and the target position are given, too.

Positrons pass by the diaphragm and are detected by a liquid-nitrogen-cooled Si(Li) detector with 5 cm diam and 5 mm depletion depth mounted at the end of the second quarter turn of the torus. Together with their annihilation radiation detected in a surrounding fourfold NaI-ring crystal they are identified as positrons.

As reported in Refs. [9,19] the energy calibration and response function determination of the Si(Li) counters is performed using electron conversion sources and continuous spectra from β^+ and β^- emitters. The β source ^{106}Ru gives an additional test of the response function up to an energy of E_{e^-}=3.54 MeV.

To extend the measurable energy range of electrons up to 8 MeV, a new detector [24] is placed in the solenoidal field opposite to the S-shaped torus. To position the detector as far away as possible from the target the solenoidal part of the spectrometer was extended by adding eight more coils to the setup. Thus, a distance of 53 cm away from the target was obtained. The magnetic field along the spectrometer axis is shown in the insert in Fig. 2. The components of the detector are sketched in Fig. 3. The energy of the electrons is measured with a 5-cm-long plastic cylinder (NE102) of 7.5 cm diam, stopping electrons up to an energy of 10 MeV. The rather poor energy resolution of $\Delta E/E$ $\approx$10% for energies above 2 MeV is tolerated in order to have the advantage of a good time resolution ($\Delta t \approx 1$ ns). To separate electrons from γ rays and neutrons, a silicon surface barrier ΔE detector of 500 μm thickness and a diameter of 7.5 cm is placed in front of the plastic block. The energy loss of electrons in the detector was calculated from [26] to be $\langle \Delta E \rangle$=210 keV for electron energies in the range from 1 to 10 MeV, taking into account the various incident angles of the electrons. By cooling the detector down to 10 °C the signal-to-noise ratio was improved significantly. The detection efficiency for γ rays was measured using radioactive sources. Including the ratio $\Omega_{e^-}/\Omega_\gamma$=122 of the solid angles for electrons transported to the detector and for γ rays, an efficiency ratio of $\varepsilon_{e^-}/\varepsilon_\gamma$ $\approx$4500 is reached. Together with a time-of-flight analysis a complete suppression of neutron events is obtained. Figure 4(a) shows the transmission to the ΔE detector measured with 365 keV electrons from a

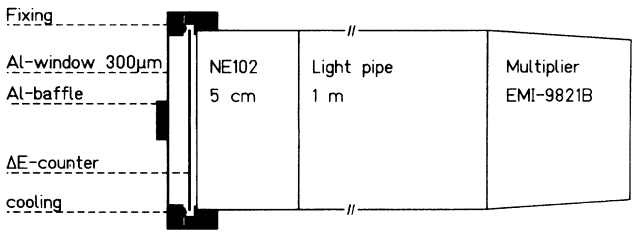

FIG. 3. Components of the plastic detector designed to measure electrons in the energy range of 2 MeV up to 8 MeV.

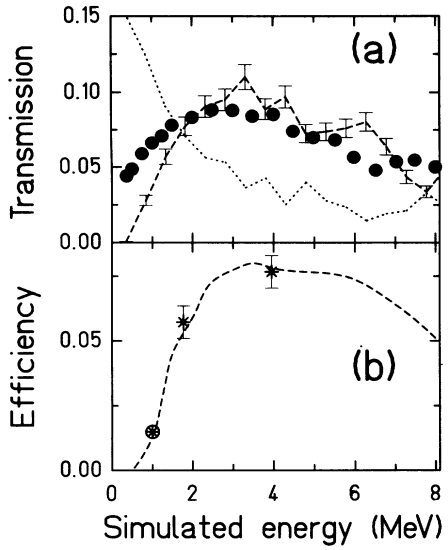

FIG. 4. Upper part: Measured (symbols) and calculated (dashed line) transmission of the plastic detector for electrons. The dotted line denotes the probability to hit the baffle, mounted in front of the detector to cut the low-energy part of the exponential δ-electron spectrum. Lower part: Detection efficiency for electrons as determined from the transmission measurement. The symbols are from measurements using the 1.0 and 1.7 MeV conversion line from a ^{207}Bi source. The data point at higher energy is obtained by reducing the magnetic strength.

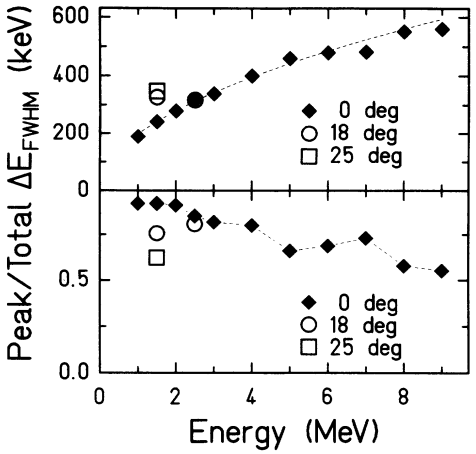

FIG. 5. Energy resolution (upper part) and peak-to-total ratio (lower part) of the plastic detector as determined from the measurement of monoenergetic electrons at the Giessen Linac. Only at low electron energies the measured values vary with increasing incident angle of the electrons.

^{113}Sn conversion source. The data points for higher energies are obtained by reducing the magnetic field, thus simulating the corresponding trajectories. The measurement is in good agreement with the transmission curve obtained by Monte-Carlo simulations [dashed line in Fig. 4(a)]. A cylindrical aluminum baffle mounted in front of the detector provides a good suppression of the very high yield of low-energy electrons, which spiral close to the magnetic axis. The dotted line in Fig. 4(a) exhibits the rate of electrons hitting the baffle. In the experiment a coincident signal in both, the ΔE counter and the plastic block, is required, which reduces the efficiency mainly at low electron energies as shown in Fig. 4(b). The symbols are measurements using the conversion electron lines of a ^{207}Bi source.

The response function of the detector setup is determined by using electrons in the energy range of 1–10 MeV delivered by the electron accelerator of the Institut für Strahlenforschung, University of Giessen, Germany. Different incident angles for the monochromatic electrons ($\Delta p/p \approx 0.5\%$) are measured in order to obtain the response function for the TORI measurements [24]. Figure 5 shows the energy resolution and the peak/total values obtained from these measurements. They are used to calculate the response function necessary for the unfolding of the measured δ-electron spectra. The measurement of the continuous spectrum of the β source ^{106}Ru (E_{max}=3.54 MeV) at the TORI spectrometer gives an additional test of the response function.

As in previous experiments [9], a pair of positron-sensitive heavy-ion counters is used to study kinematical coincidences by measuring the angles of the outgoing fragments and to distinguish sequential fission events from scattered heavy ions. These parallel-plate avalanche detectors (PPAC) work with a delay-line technique. The delay lines are read out on both sides in order to recognize double-hit events. These originate from cases where one reaction partner (three-body events) or both reaction partners undergo fission (four-body events). Events where one or two fission fragments do not hit the counters, are distinguishable from true three- and four-body events by the energy-loss signal of the counters as the energy-loss signal from a fission fragment is much lower than the signal obtained from one heavy reaction partner or two fission fragments hitting the counter simultaneously. The scattering angles are calculated from the position information of the particle counters. Because the PPAC are only 5.5 cm away from the target the total kinetic-energy loss (TKEL) of the reaction cannot be obtained from a time-of-flight analysis. It is obtained from the scattering angles calculated from the hit position as explained in Sec. III A.

To extend the detection range for scattered ions a photodiode array [25] is placed between the PPAC. It allows the detection of scattered particles in the scattering angle range of $6° \leq \vartheta \leq 10°$ and to discriminate fission fragments from elastically scattered Pb ions.

For high TKEL values a significant amount of the measured electrons originate from nuclear processes. These contributions have to be subtracted because only the atomic part of the spectra contains the information on the nuclear trajectories. To determine the contribution of leptons from nuclear origin, the γ-ray spectra are measured with a 10 cm×15 cm BaF_2 crystal. The γ detector is mounted perpendicular to the beam axis leading to maximum Doppler broadening without a significant mean Doppler shift. Like for the plastic detector, the good time resolution of the BaF_2 crystal is necessary

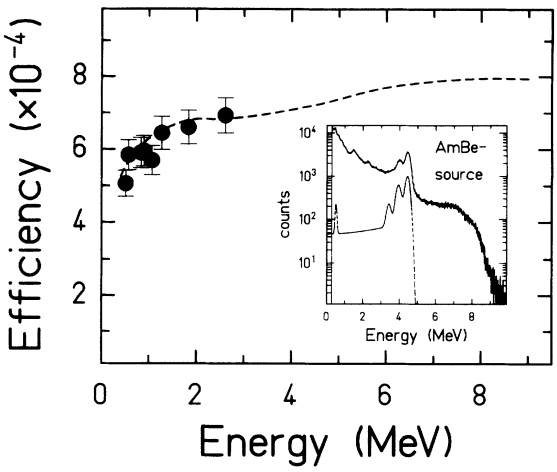

FIG. 6. Measured (symbols) and calculated (dashed line) total detection efficiency of the BaF_2 detector for monoenergetic γ rays. The insert shows the spectra obtained with an AmBe source. The response function for 4.4 MeV γ rays is shown as well.

to separate γ rays from neutrino-induced background events. In order to determine the nuclear background up to energies of 8 MeV the γ spectrum was measured up to 9 MeV. The efficiency and the response function for these high energies—the highest γ transition suitable for determining the response function is the 4.4 MeV line delivered by an AmBe source—was obtained from a Monte Carlo simulation based on the GEANT III program package [27]. The efficiency of the BaF_2 detector was shown in Fig. 6. The data points are measurements obtained with conventional γ sources. The dashed line denotes the result of the GEANT simulation, taking into account the TORI geometry and the surrounding material. The insert of Fig. 6 shows the spectrum obtained with the AmBe source, exhibiting the 4.4 MeV line and the single escape peak on a huge background of neutron events. The analytical response function for 4.4 MeV γ rays is shown by the dashed curve. A PuC source is additionally used to deliver a calibration point at 6.13 MeV.

III. DATA ANALYSIS

A. TKEL and impact parameter determination

Dissipative collisions are characterized by a massive mass transfer and dissipation of collective kinetic energy into intrinsic excitation energy. For the symmetric Pb+Pb system the net mass transfer is zero and the total kinetic-energy loss (TKEL) can then be calculated from the deviation of the sum of the primary laboratory scattering angles from 90° in the laboratory system. Monte Carlo studies including mass transfer [28] and neutron evaporation yield a TKEL resolution of $\sigma \approx 100$ MeV for binary events. In the case one partner (three-body events) or both scattering partners (four-body events) undergo sequential fission the primary scattering angles are still well defined ($\tau_{\text{fiss}} \approx 10^{-20}$ s [29]), but due to neutron evaporation and systematic errors in reconstructing the primary scattering angles for fission events the TKEL resolution becomes $\sigma \approx 200$ MeV. For the four-body event class no cuts in TKEL can be applied any more. In the case one partner undergoes fission it can happen that one fission fragment does not hit the detector and, in spite of an additional check of the energy-loss signal, will be erroneously identified as a two-body event. For both the two- and three-body cases these events appear mainly at high TKEL values and can be separated by setting windows in the (TKEL, ϑ) distribution. These windows are chosen with the help of Monte Carlo studies. The contribution of falsely identified three-body events in the highest TKEL window applied to two-body events amounts to less than 1%. For the class of three-body events the situation appears to be more difficult because in the case that both partners undergo fission it is very unlikely that all fragments are detected. Thus only these events where the targetlike partner had fissioned—which can clearly be distinguished in the $(\Delta E, \vartheta)$ matrix—are accepted as true three-body events. For the windows selected the contribution of wrongly identified four-body events amounts also to less than 1%.

To compare the measured δ-electron spectra with theoretical predictions, the impact-parameter distributions must be known. This is achieved using a Monte Carlo simulation of the experiment as described in detail in Ref. [9]. The deflection function predicted by the trajectory models discussed below is used as an impact to simulate the acceptance of the particle counters. The calculation takes into account the influences of the target thickness, charge states of the outgoing particles, deflection of the particles in the magnetic field, mass transfer, the fission probability, and particle evaporation, as well as the geometrical boundaries of the particle counters and their position and energy-loss resolution. The data obtained with the simulation undergo the same analysis as the experimental ones. By this procedure the same (TKE,ϑ) distributions as in the experiment are obtained. Figure 7 shows the measured and the simulated (TKE,ϑ) distribution for binary and three-body events. For the simulated data the impact parameters are stored in a third dimension. Applying cuts in the simulated (TKE,ϑ) matrix yields the impact-parameter distributions corresponding to the selected events. These distributions are used to calculate the δ-electron spectra which are compared with the measured ones obtained when applying the same cuts in the experimental distribution. The influences of the limited position, energy loss, and TKEL resolution and the probability of wrong event-class assignment is accounted for within this procedure. The windows applied are depicted in Fig. 7.

As discussed in the introduction a prolonged interaction time leads to pronounced minima in the spectral distribution of δ electrons. These minima are smeared out due to the loss of kinetic energy during the collision and furthermore by statistical fluctuations of the frictional force. They lead to a distribution of interaction times even for a fixed impact parameter [9,15]. From this it becomes clear that even if the experimental data would allow the selection of small impact-parameter

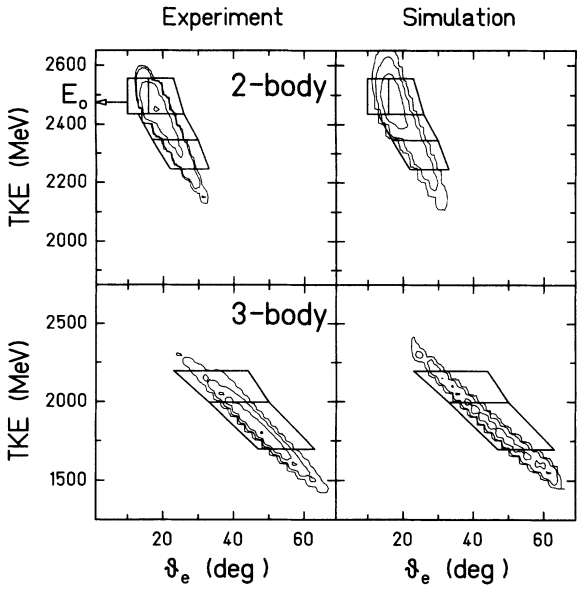

FIG. 7. Experimental (left part) and simulated (right part) (TKE,ϑ_e) distribution for the system Pb+Pb at 12 MeV/nucleon incident energy for two event classes. The two-dimensional windows applied to these distributions are depicted as well.

regimes (which is not the case due to the limited TKEL resolution) the statistical fluctuations lead to a smearing out of the oscillatory structures. When comparing the measured δ-electron spectra with the theoretical predictions, both the limited TKEL resolution and the statistical fluctuations have to be taken into consideration. The reaction-model calculations give a mean TKEL(b) dependence resulting from the calculation of the mean trajectory for a given impact parameter. The experimental TKEL resolution is accounted for in the Monte Carlo simulation and leads to a distribution of impact parameters even when selecting small TKEL regimes. As shown in Ref. [9] the influence of the statistical fluctuations on the spectral distribution of δ electrons can be accounted for by an additional broadening of the impact-parameter distribution used to calculate the theoretical δ-electron spectra. The additional width is calculated using the $\tau(b)$ dependence predicted by reaction-model calculations and using $\delta\tau/\tau \approx 1$ as estimated from the experimental data [9] and confirmed by the calculations of Ref. [15]. For the comparison of the experimental and theoretical δ-electron spectra presented in this work the influence of the statistical fluctuations on the spectral shape can be neglected. Only when selecting events corresponding to TKEL values above 200 MeV is an indication for a prolonged contact time found in the δ-electron spectra. These high TKEL values correspond to events where one partner fissioned. The experimental TKEL resolution for these events is $\sigma \approx 200$ MeV, thus leads already to a broad impact-parameter distribution. Furthermore, applying a 300 MeV broad window in TKEL the selected impact-parameter distribution becomes broad enough to mask the influence of the statistical fluctuations.

B. Determination of the nuclear contribution

To compare the measured distributions of δ electrons with the theoretical predictions for the atomic δ-electron spectra the lepton spectra originating from nuclear conversion processes must be subtracted. They are determined by converting the unfolded and efficiency-corrected γ-ray spectra, measured under the same conditions, into leptons using theoretical conversion coefficients. A contribution of electrons and positrons originating from nuclear E0 transitions cannot be determined by this procedure. These transitions do not show up in the γ-ray spectra but will cause an excess of positrons and electrons above the combined atomic and nuclear contribution.

Before starting the conversion procedure, a multipolarity decomposition of the γ-ray spectra must be performed as the conversion coefficients depend on the transition type. As pointed out by Refs. [30,31], the γ-ray spectrum following ($HI, xn\gamma$) reactions is well understood as a mixture of E1/E2 transitions at γ-ray energies above 1 MeV. This observation is confirmed by the examinations of collision systems where only positrons of nuclear origin are detected [6,9,32,33]. It has been shown that the measured positron spectra are well explained assuming that the high-energy part of the spectra contains predominantly E1 transitions whereas the low-energy part, which can be described by an exponential distribution, is caused by collective E2 transitions. This procedure is an established tool used for the determination of the atomic positron production probability in heavy-ion collisions [34,35]. Taking into account an admixture of magnetic dipole transitions (M1) does not alter the result of the conversion procedure. For heavy nuclei in the $Z \geq 80$ regime and transition energies above 1 MeV the pair conversion coefficients are nearly the same for E2 and M1 transitions [36].

At the high-energy part a statistical E1 distribution of the form

$$\frac{dN}{dE_\gamma} = \left(\frac{E_\gamma}{P_3}\right)^{P_1/P_2} \exp\left(\frac{-E_\gamma}{P_2}\right) \qquad (2)$$

was fitted to the spectra [27]. The three parameters determine the position of the maximum of the distribution ($P_1 \approx 1.2$ MeV), the slope (usually considered as a temperature; $P_2 \approx 400$–600 keV), and the height of the distribution (P_3). To account for the limited statistics at high γ-ray energies a maximum-likelihood fit was applied.

As an example the γ-ray spectra for two TKEL regimes are shown in Fig. 8. The spectra are corrected for efficiency and detector response. The statistical E1 and the E2 distribution are shown by the dashed and the dashed-dotted lines, respectively. For the conversion procedure the theoretical conversion coefficients of Refs. [36,37] are used. The Z dependence of the conversion coefficients was taken into account by assuming nuclei with Z=82 in the case of two-body collisions and a mixture of Z=41 (67%) and Z=82 (33%) for the case where one particle undergoes fission (three-body events).

The validity of the multipolarity decomposition is con-

trolled by converting the γ spectra into positron spectra using the double-differential pair conversion coefficients of Ref. [36]. The nuclear positron spectra are then compared with the measured positron spectra. This procedure is very accurate for high TKEL values where only a small fraction of positrons ($\lesssim$10%) originate from atomic processes [9]. Figure 8(b) shows the positron spectra for the same TKEL ranges as the γ-ray spectra depicted in Fig. 8(a). The nuclear contributions are depicted by the dotted lines. The dashed lines show the sum of nuclear and atomic contributions. The shape and the height of the nuclear contribution is very sensitive to the multipolarity mixing. An overestimation of the E1 part leads to an overestimation of the nuclear contribution, especially in the energy range above 1 MeV where more than 95% of the measured positrons are of nuclear origin. The underestimation of the measured positron yield visible below 750 keV in the spectrum for the lower TKEL window is the subject of a separate publication dealing with an observed excess of positrons already in elastic collisions [38].

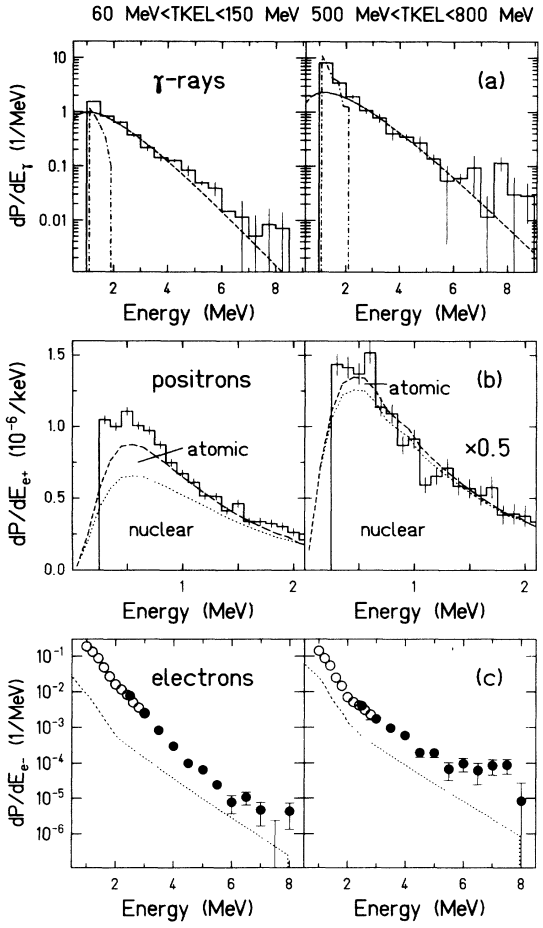

FIG. 8. Determination of the nuclear part of the electron spectra for Pb+Pb at 12 MeV/nucleon incident energy. (a) γ-ray spectra for two kinematical regimes together with the assumed multipolarity decomposition (dashed curve: statistical E1 distribution; dash-dotted curve: remaining E2 part). (b) Measured positron spectra with calculated nuclear (dotted curve) and added atomic contribution (dashed curve). The agreement at energies above 1 MeV confirms the multipolarity assignment. (c) Measured electron spectra and calculated nuclear contribution (dotted curve). Different data symbols are used to distinguish the data points from the Si(Li) array (low-energy part) and the plastic detector (high-energy part).

Figure 8(c) shows the δ-electron spectra together with the nuclear contribution calculated from the γ spectra displayed in the upper part of Fig. 8. The uncertainty in the determination of the high-energy lepton spectra is mainly due to the limited statistics at the high-energy end of the γ spectra. It is estimated using the procedure described in the following. The statistical E1 distribution fitted in the energy range between 3 and 6 MeV decreases faster towards higher energies than an exponential function fitted in the same energy range. The assumption of an exponential decrease of the high-energy spectra gives an upper estimate for the statistical E1 yield. While at γ energies of 5 MeV the exponential fit gives the same yield as the statistical distribution it exceeds the latter one by a factor of 1.5 at energies above 8 MeV. From this an error of 50% in the determination of the nuclear background at 8 MeV is concluded. Different data symbols are used for the δ electrons measured with the Si(Li) counters and the new plastic detector. They overlap in the region of 2–3 MeV. Before comparing the δ-electron spectra with the theoretical predictions the nuclear contribution is subtracted.

IV. ELASTOPLASTICITY IN DISSIPATIVE COLLISIONS

A. The dissipative diabatic model

For the description of the nuclear trajectories we start out from the microscopic semiclassical one-body dissipation model as explained in detail in Ref. [17]. Without adjustable parameters this model describes a large body of experimental data on nucleus-nucleus collisions [12,39]. Its friction coefficients are calculated microscopically, based on the ideas of the window and wall dissipation [21]. In particular, for the system Pb+Pb at an incident energy of 8.6 and 12 MeV/nucleon [9,20], the δ-electron spectra up to 3 MeV are well accounted for within the one-body dissipation model. The observed long contact times are caused by the formation of a pronounced neck in the outgoing phase of the reaction. In the early stage of the collision the one-body dissipation model predicts a very fast deceleration (although still too slow compared to the experimental result of this paper) which is in contradiction to the Markov assumption implied in this and all other friction models. Indeed, the radial deceleration time $\tau_{\rm decel}$ is about 0.2×10^{-21} s (cf. Fig. 1) while the thermal equilibration time $\tau_{\rm therm}$ is about $(0.2 \times 10^{-21}\ {\rm MeV\,s})/\epsilon^*$, where ϵ^* denotes the excitation energy per nucleon [40]. Since ϵ^* varies typically between 0 and 1 MeV in these collisions, $\tau_{\rm decel} \lesssim \tau_{\rm therm}$ during the whole deceleration phase which has the consequence that during the deceleration the dissipation process is essentially non-Markovian. By measuring high-

energy δ electrons up to 8 MeV one is sensitive to time scales of the order of a few 10^{-22} s, and hence memory effects can be investigated. Such memory effects have been extensively studied within the diabatic approach to dissipative collective nuclear motion [22]. This theory of dissipative diabatic dynamics is closely related to the microscopic one-body dissipation model. Therefore, it is possible to obtain a dissipative diabatic model from the one-body dissipative model by introducing only the memory time as an additional quantity.

In the one-body dissipation model the macroscopic variables q_i of the nuclear system consist of three shape degrees of freedom and three rotational angles: $q_1 = s$ distance between the centers of the two nuclei, $q_2 = \sigma$ neck and deformation, $q_3 = \Delta$ shape asymmetry (always =0 for symmetric collisions), $q_4, q_5, q_6 = \theta, \theta_1, \theta_2$ angles of rotation. For a detailed definition see Ref. [17]. The equations of motion for these variables are governed by an adiabatic potential $V(q_1, q_2, q_3)$ which includes the nuclear and Coulomb interaction, a mass tensor $M_{ij}(\mathbf{q})$, and the friction force F_i^{Markov} which is given by

$$F_i^{\text{Markov}} = -\sum_{j=1}^{6} \gamma_{ij}(\mathbf{q})\dot{q}_j. \tag{3}$$

In this expression $\gamma_{ij}(\mathbf{q})$ denotes the one-body dissipation friction tensor and $\mathbf{q} = \{q_1, \ldots, q_6\}$.

Guided by the importance of diabatic single-particle motion in dissipative heavy-ion collisions we have replaced the Markovian friction force in Eq. (3) for the shape degrees of freedom $q_1 = s$ and $q_2 = \sigma$ by a retarded friction force F_i as introduced in Ref. [22]. Its components are determined by the differential equations

$$\frac{dF_i}{dt}(t) = -\lambda_{\text{intr}}(t)F_i(t) - \sum_{j=1}^{2} C_{ij}[\mathbf{q}(t)]\dot{q}_j(t)$$

$$\text{for } i = 1, 2, \tag{4}$$

where $\lambda_{\text{intr}}(t)$ and C_{ij} denote the intrinsic equilibration rate (inverse memory time) and the stiffness tensor, respectively. Since the rotational degrees of freedom do not influence the shape of the nuclear system, which means that the potential does not depend on the angles, one does not expect a strong diabatic effect in these variables. Therefore, q_4, q_5, and q_6 are treated within the usual Markovian approximation (q_3=0 for the symmetric system considered in this work).

In the limit of small λ_{intr}, such that the first term on the rhs of Eq. (4) can be neglected, one obtains the elastic limit in which the force is given by the contour integral

$$F_i^{\text{elastic}}(t) = -\oint^{\mathbf{q}(t)} \sum_{j=1}^{2} C_{ij}(\mathbf{q})dq_j \quad \text{for } i = 1, 2. \tag{5}$$

Since it neither depends explicitly on time nor on $\dot{q}_i$, it is conservative. In this case the collective motion is elastic without any dissipation.

In the opposite limit of large λ_{intr}, such that $F_i(t)$, $C_{ij}[\mathbf{q}(t)]$, and $\dot{q}_j(t)$ do not change considerably during time intervals of the order $\lambda_{\text{intr}}^{-1}$, dF_i/dt can be neglected in Eq. (4), and hence, in this Markovian limit, the force can be written as

$$F_i^{\text{Markov}}(t) = -\sum_{j=1}^{2} \frac{C_{ij}[\mathbf{q}(t)]}{\lambda_{\text{intr}}(t)}\dot{q}_j(t) \quad \text{for } i = 1, 2, \tag{6}$$

i.e., a pure friction force.

For intermediate values of λ_{intr}, the system behaves like a damped oscillator with a frequency-dependent friction coefficient. The elastic response on fast deformations and the dissipative response on slow deformations is typical for elastoplastic materials like glass, glycerine, and "Silly Putty" (a plastic toy).

There is a close relationship between dissipative diabatic dynamics and the one-body dissipation model. Both approaches are based on the same microscopic picture which determines the collective motion for the distortion of the nucleonic Fermi distribution by the time-dependent shapes of the nuclear system. This coupling between intrinsic and shape degrees of freedom yield the stiffness tensor C_{ij} in the diabatic approach and it provides the friction tensor γ_{ij} in the one-body dissipation model via the additional assumption that the distortions in the nucleonic momentum distribution relax instantaneously. Indeed, for the quadrupole motion of a cube of matter the stiffness parameter C is related to the friction coefficient γ in the one-body dissipation model (wall formula) by [22]

$$C = \frac{24}{5}\frac{2}{9}\frac{\gamma}{\tau_{sp}} \approx \frac{\gamma}{\tau_{sp}}, \tag{7}$$

where τ_{sp} denotes the time of flight of a nucleon with Fermi velocity v_F through the cube. In defining the dissipative diabatic model, we assume the general validity of this relation in the form

$$C_{ij}(\mathbf{q}) = \alpha\frac{\gamma_{ij}(\mathbf{q})}{\tau_{sp}} \tag{8}$$

with $\tau_{sp} = 2R_0/v_F$ and $R_0 = 1.2$ fm$\times(A_1 + A_2)^{1/3}$ being the radius of the compound nucleus. Here, a parameter α is introduced to correct for shortcomings of the simple cube model with respect to realistic shapes, single-particle potentials and effective nucleon mass m_{eff}. According to the microscopic expression [22,49], the stiffness tensor C_{ij} is proportional to $m_{\text{eff}}^{-5/2}$ and to the level density which experimentally is twice as large as the Fermi-gas value. Since in the simple cubic model γ_{ij}/τ_{sp} in Eq. (7) is deduced from the Fermi-gas model with $m_{\text{eff}} = m_{\text{nucleon}}$, we expect $\alpha \approx 2m_{\text{eff}}^{-5/2}$ which yields $\alpha \approx 5$ for a realistic value of $m_{\text{eff}} = 0.7m_{\text{nucleon}}$. Furthermore, compression is not allowed in the collective model, and hence we expect even larger values (larger by roughly a factor of 2 corresponding to $\alpha \approx 10$) for the stiffness coefficient to be effective in the approach phase.

For the intrinsic equilibration rate $\lambda_{\text{intr}}(t)$ we consider three major contributions,

$$\lambda_{\rm intr}(t) = \lambda_2(t) + \lambda_x + \lambda_a(t). \tag{9}$$

(i) The first term results from two-body collisions and is estimated by Bertsch [40] as $\lambda_2(t) = \epsilon^*(t)/t^*$ where $\epsilon^*(t) = E_{\rm intr}(t)/A$ denotes the excitation energy per particle and the parameter $t^* = 0.2 \times 10^{-21}$ MeV s. The total conserved energy $E_{\rm tot}$ of the system is composed of the collective kinetic energy, the adiabatic potential energy $V(\mathbf{q})$ and the excitation energy $E_{\rm intr}$:

$$E_{\rm tot} = \frac{1}{2}\sum_{k,l=1}^{6} \dot{q}_k(t) M_{kl}[\mathbf{q}(t)]\dot{q}_l(t) + V[\mathbf{q}(t)] + E_{\rm intr}(t). \tag{10}$$

Thus, the excitation energy $E_{\rm intr}$ is given by

$$E_{\rm intr}(t) = -\int_{-\infty}^{t} dt' \sum_i F_i(t')\dot{q}_i(t') \tag{11}$$

and includes all energy which is neither in the adiabatic potential $V(\mathbf{q})$ nor in the collective kinetic energy.

(ii) Since the mean-field couples the diabatic states there is a certain probability that the particles do not follow the diabatic states at the crossings but jump to the other states which can be lower in energy (mainly in the approach phase) or also energetically higher (mainly during the rupture of the neck close to the scission line). In any case these single-particle transitions lead to a decay of the diabatic friction force F_i in Eq. (4). The according rate λ_x is given in Ref. [41] as $2\pi|H'|^2/\hbar\delta_x$ with H' the mean coupling matrix element between the diabatic states and δ_x the mean distance in energy between crossings along a diabatic level. For realistic values $\delta_x \approx 2$ MeV and $H' \approx 0.5$ MeV we obtain $\lambda_x \approx 1.25 \times 10^{21}$ s^{-1}.

(iii) The time dependence of the diabatic wave functions includes deformations which can be described by a velocity field. Variations which are due to accelerations in the mean-field Hamiltonian are not incorporated and lead to additional couplings between diabatic states. The last term λ_a accounts for this effect. From the golden rule and the microscopic expression given in Ref. [42] for the coupling Hamiltonian we obtain

$$\lambda_a = \beta\,(\ddot{q}_1)^2 (10^{-21}\ \text{s})^3\ \text{fm}^{-2}.$$

Using a mean absolute value of $0.2R_0|\dot{q}_1|$ for the single-particle matrix element of the velocity potential the parameter β is estimated to be about 0.1.

Altogether the following equations of motion are solved in the dissipative diabatic model:

$$\frac{d}{dt}\left(\sum_{j=1}^{6} M_{ij}(\mathbf{q})\dot{q}_j\right) = \frac{1}{2}\sum_{j,k=1}^{6} \dot{q}_j \frac{\partial M_{jk}(\mathbf{q})}{\partial q_i}\dot{q}_k - \frac{\partial V(\mathbf{q})}{\partial q_i} + F_i(t). \tag{12}$$

The diabatic friction forces $F_1(t)$ and $F_2(t)$ are given by the differential equation (4) ($F_3 = 0$ for symmetric systems) while the Markovian friction forces for the rotational degrees of freedom are taken from the one-body dissipation model as

$$F_i = -\sum_{j=4}^{6} \gamma_{ij}(\mathbf{q})\dot{q}_j \quad \text{for } i = 4,5,6. \tag{13}$$

B. Illustration of the elastoplastic response

In the following the nuclear trajectories for central collisions of Pb+Pb obtained with the new dissipative diabatic model will be discussed to illustrate the elastoplastic properties and to show the sensitivity of the trajectories and of the δ-electron spectra on the estimated parameters which enter the stiffness tensor C_{ij} and the intrinsic equilibration rate $\lambda_{\rm intr}$. For this, mainly an energy of 8.6 MeV/nucleon will be considered since higher incident energies would lead to larger excitation energies already at the first stage of the collision so that the intrinsic equilibration rate [Eq. (9)] would be dominated too much by the term $\lambda_2 = \epsilon^*/t^*$, losing the sensitivity on the term λ_a. This can be understood by the following simple considerations on the correlations between beam energy, energy loss, and interaction time.

In the one-body dissipation picture for peripheral collisions the energy loss is proportional to the available energy $E_{\rm av}$ at the Coulomb barrier V_c, $E_{\rm av}$=TKE$-V_c$, and the number of exchanged nucleons, $N_{\rm ex}$, according to

$$-dE_{\rm av} = \frac{E_{\rm av}}{\mu} dN_{\rm ex}, \tag{14}$$

where μ denotes the reduced mass of the system [43,44]. Assuming that for a small number of exchanged particles, $N_{\rm ex}$ is about proportional to the interaction time $t_{\rm int}$ (random walk diffusion) one sees that the same

$$\text{TKEL} = -\int dE_{\rm av} \sim E_{\rm av} t_{\rm int}$$

implies a much shorter interaction time for the beam energy of 12 MeV/nucleon than for 8.6 MeV/nucleon which is only 3 MeV above the Coulomb barrier. This correlation is seen in the result of the one-body dissipation

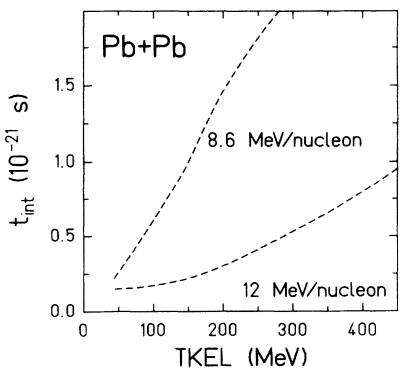

FIG. 9. Relation between the nuclear interaction time and the total kinetic-energy loss (TKEL) for collisions of Pb+Pb at 8.6 and 12 MeV/nucleon as predicted by the one-body dissipation model.

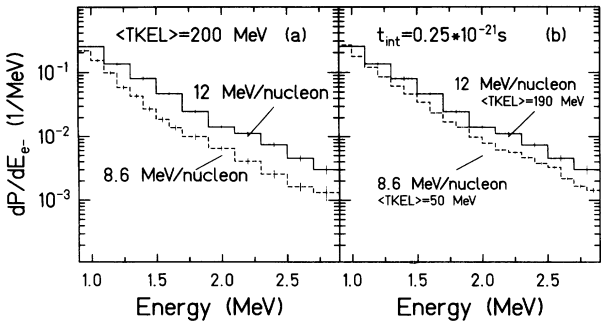

FIG. 10. Comparison of the δ-electron spectra measured for Pb+Pb collisions at 8.6 MeV/nucleon (dashed line) and 12 MeV/nucleon (solid line). The spectra shown in the left part correspond to collisions with the same TKEL bin. The same slope of the spectra (right part) can only be obtained by selecting different TKEL regimes for the 8.6 and 12 MeV/nucleon data, respectively.

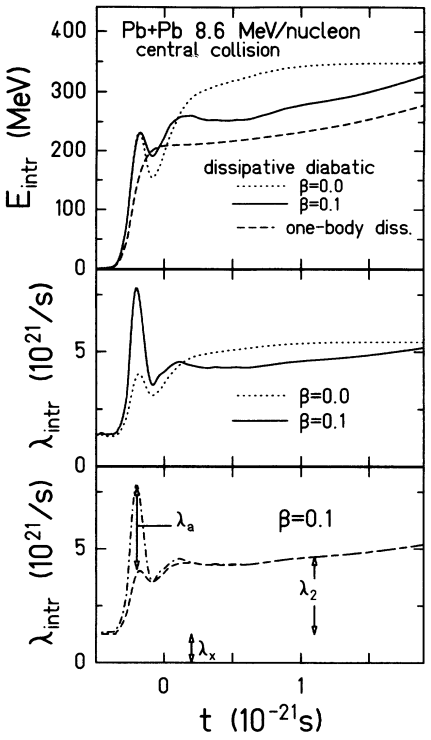

FIG. 11. Time evolution of the intrinsic excitation energy predicted by the one-body dissipation model and the dissipative diabatic model for two different values of the β parameter (upper part). The middle part exhibits the corresponding intrinsic equilibration rate. The lower part shows the time evolution of the three contributions to the total equilibration rate.

model in Fig. 9 and in the measured δ-electron spectra displayed in Fig. 10. If one chooses the same TKEL bin around 200 MeV [Fig. 9 (left part)] the slopes of the spectra below 1.8 MeV differ and indicate a longer interaction time for a beam energy of 8.6 MeV/nucleon than for 12 MeV/nucleon. According to the prediction shown in Fig. 9 an interaction time of $t_{\rm int} = 0.25 \times 10^{-21}$ s corresponds to TKEL=50 and 190 MeV for the two bombarding energies, respectively. The δ-electron spectra displayed in Fig. 10 (right part), which have been measured in coincidence with these TKEL values, have indeed a similar slope in contrast to Fig. 10 (left). This confirms nicely the expected correlations between beam energy, TKEL, and interaction time.

Figure 11 shows in the upper part for a head-on collision the time evolution of the intrinsic energy which is given by Eq. (11). In the case of the one-body dissipation model which assumes instantaneous equilibration (dashed line in Fig. 11) the excitation energy is of a thermal nature and has to increase monotonically in time. Compared to this, the dissipative diabatic model shows a faster increase of the intrinsic energy, because a large fraction of the initial kinetic energy is stored into a diabatic potential, which, according to Eq. (4), is built up at the beginning of the collision. This energy is partially transformed back into collective motion as seen in the upper part of Fig. 11 by the decrease of the intrinsic energy after the turning point which is at $t = -0.2 \times 10^{-21}$ s (cf. also Fig. 12). A larger feedback into collective kinetic energy is prevented by the relaxation of the diabatic potential into thermal excitations.

The corresponding relaxation rates calculated from Eq. (9) are shown for two different cases in the center part of Fig. 11. At the beginning of the collision where the deceleration is largest, the acceleration component

$$\lambda_a = \beta\,(\ddot{q}_1)^2 (10^{-21}\ \mathrm{s})^3\ \mathrm{fm}^{-2},$$

of the intrinsic equilibration rate leads to a rapid decay of the diabatic potential and thus reduces the amount of energy which is transferred back into collective motion. In the lower part of Fig. 11 the total relaxation rate is decomposed into its three contributions according to Eq. (9) for the case of β=0.1 and $t^* = 0.2 \times 10^{-21}$ MeV s. One sees that λ_a which is due to accelerations contributes most strongly in the first 0.3×10^{-21} s of the collision. The decay rate λ_2 caused by two-body collisions also grows rapidly during this short time period as it is proportional to the excitation energy per particle $\epsilon^* = E_{\rm intr}/A$ which includes the energy stored in the diabatic potential. After a short decrease, which reflects the fact that part of the diabatically stored energy has been fed back into relative motion, its further increase is only minor because almost all kinetic energy has already been transformed into thermal excitations and the system can gain additional excitation energy only from shape deformations which lower the Coulomb energy at the expense of surface energy. The decay rate λ_x, which comes about by the coupling of the diabatic states at the crossings, is the smallest contribution and is for simplicity assumed to be independent on the macroscopic variables.

Figure 12 shows the time evolution of the nuclear distance in terms of twice the rms radius $R(t)$ of the nuclear charge distribution. In Fig. 12(a) the parameter β has been varied to study the influence of the equilibration rate λ_a caused by collective accelerations. Neglecting the term λ_a (i.e., $\beta = 0$) results in a fast reseparation

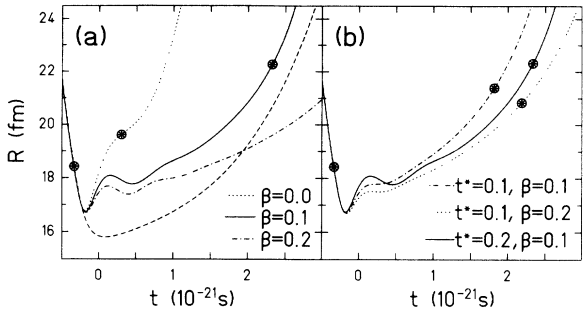

FIG. 12. Time evolution of the nuclear distance in times of twice the root-mean-square radius of the nuclear charge distribution for central collisions of Pb+Pb at 8.6 MeV/nucleon incident energy (dashed line: one-body dissipation model, broken and solid lines: dissipative diabatic model with α=10). Part (a) shows trajectories obtained with $t^* = 0.2 \times 10^{-21}$ MeV s and different values of the parameter β. In (b) t^* (in units of 10^{-21} s) and β are varied to show the sensitivity on the relaxation rates λ_2 and λ_a. The spoke-wheel symbols denote the instants where the surfaces of the two nuclei touch and where the neck ruptures. The time in between is regarded as the nuclear interaction time $t_{\rm int}$. For the one-body dissipation model and the dissipative diabatic picture with β=0.2, the neck rupture occurs at times later than 3×10^{-21} s.

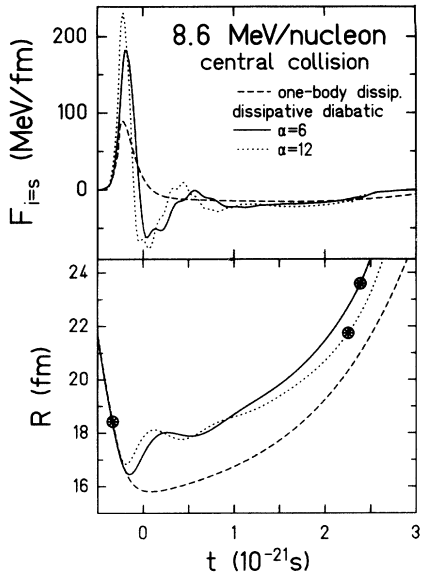

FIG. 13. Time evolution of the radial friction force (upper part) and nuclear trajectories (lower part) in terms of twice the root-mean-square radius of the nuclear charge distribution (dashed line: one-body dissipation model; dotted and solid lines: dissipative diabatic model with different values of the parameter α.) The spoke-wheel symbols denote the instants of touching and rupture of the two surfaces.

of the nuclei. Although the diabatic force, which is built up with increasing R [i.e., $\dot{R} > 0$, cf. Eq. (4)], strongly decelerates the separation, it is not large enough to push the nuclei towards each other again. The additional decay rate λ_a with $\beta \approx 0.1$ (theoretical estimate) during the initial deceleration phase is necessary to obtain the inward reflection (cf. the solid lines in Figs. 12 and 13). After the initial fast stopping the neck can develop and the opening up of this degree of freedom brings the nuclear system into the dissipative regime where the motion is slow compared to the relaxation rates. As can be seen from the bottom part of Fig. 11, λ_a has dropped to zero at about $t = 0.2 \times 10^{-21}$ s and all subsequent relaxation is due to the two-body collisions and the decay at the crossings. A typical time scale for the collective variable during this slow motion part of the dynamical evolution is $\approx 0.6 \times 10^{-21}$ s and the inverse of the total relaxation rate is $\lambda_{\rm intr}^{-1} \approx 0.2 \times 10^{21}$ s, which means that the Markov assumption is fulfilled. From the dissipative limit of Eq. (4), which is given in Eq. (6), one sees that in this regime the friction tensor $C_{ij}/\lambda_{\rm intr}$ depends directly on the parameter t^* which enters $\lambda_2 = \epsilon^*/t^*$. The trajectories displayed in Fig. 12(b) show that the smaller value $t^* = 0.1 \times 10^{-21}$ MeV s leads to a shorter nuclear contact time. The reason is that the friction force is reduced by about 30% for $t > 2 \times 10^{-21}$ s (cf. the bottom part of Fig. 11). However, increasing β to 0.2 and thus changing the initial conditions for the entrance into the dissipative regime has the same effect on the contact time as can be seen in Fig. 12(b). Because of the neck degree of freedom the situation is more intricate than, for example, in Ref. [45] where using only one collective variable a smaller t^* led to longer contact times.

Figure 12 also shows that in comparison with the one-body dissipation model the dissipative diabatic calculation exhibits a faster stopping of the nuclei followed by damped oscillations of the nuclear trajectory. The influence on the δ-electron spectra can be estimated easily without doing the coupled-channels calculation. Just keeping in mind that according to the approximate relation given in Eq. (1) the Fourier frequencies of $\dot{R}/R$ represent the energies of the δ electrons. From Fig. 12 one estimates a time period of the oscillation of $T \approx 0.6 \times 10^{-21}$ s which corresponds to an energy of $E_{\rm osc} = 2\pi\hbar/T \approx 7$ MeV. From these considerations it is evident that the initial fast stopping together with the subsequent damped oscillation is responsible for the high-energy part of the δ-electron spectrum (cf. the discussion in Sec. IV C).

In Fig. 13 we illustrate the sensitivity of the trajectories on the parameter α which has been estimated to be around 5. In the upper part the time dependence of the Markovian and the retarded friction forces acting on the relative motion is shown. Due to the retardation of the friction force, a large repulsive potential (proportional to α) is built up in the approach phase which leads to a much faster deceleration than predicted by the one-body dissipation model. As can be seen in Fig. 13 from two calculations with different values of the parameter α (i.e., different strengths of the stiffness tensor C_{ij}) the retarded friction force does not scale linearly with this parameter. Higher values of the parameter α result in a faster deceleration, and as a consequence the equilibration rate $\lambda_{\rm intr}$ is increased due to the term λ_a in Eq. (9) which leads to a faster decay of the diabatic potential [see Eq. (4)]. Thus,

the dynamical dependence among the various quantities renders a complex system where doubling of C_{ij} does not imply a twice stronger friction force F_i as would be the case in a Markovian description. However, in the lower part of Fig. 13 the corresponding nuclear trajectories show clearly that with larger values of the parameter α (and hence of C_{ij}) the frequency of the oscillation in the rms radius is increased as $\omega = (C_{ss}/M_{ss})^{1/2}$ with M the irrotational mass and C the stiffness coefficient. As in Fig. 1, which is for a beam energy of 12 MeV/nucleon, the elastoplastic response of the nuclei manifests itself in a fast stopping followed by a damped giant vibration. For more peripheral collisions the effect is not as pronounced but still present and essential for explaining the enhanced yield in the high-energy part of the δ-electron spectrum (cf. Fig. 17). The instants of touching and separating shapes, which are marked by the spoke-wheel symbols, indicate that in the dissipative diabatic calculation the nuclear contact time depends only weakly on the parameter α.

At the later stage of the collision processes the retarded friction force becomes similar to the one-body friction force. This is not accidental, because the motion becomes slow and overdamped with $f_i = \partial V/\partial q_i$ independent of the model for the dissipation process.

The atomic time $t_{\rm ato}$ is defined as the time difference between the points of closest approach of two different Rutherford trajectories, of which the first is matched with the incoming trajectory and the second coincides for large separations with the outgoing nuclear trajectory. This definition is similar to the definition of a sticking time given in the "atomic clock model" [46].

In the δ-electron spectra the atomic time is reflected by the first minimum which comes about by a destructive interference between the contributions of the incoming and the delayed outgoing part of the trajectory to the amplitude a_{if} [cf. Eq. (1)]. Figure 14 shows for a single trajectory with impact parameter b=5 fm the δ-electron spectra for collisions of Pb+Pb at 8.6 MeV/nucleon incident energy obtained with different choices of the parameters α and β.

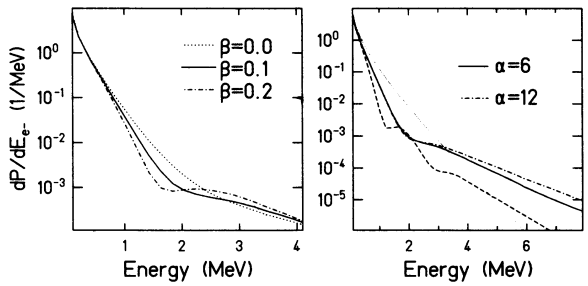

FIG. 14. δ-electron spectra for collisions of Pb+Pb at 8.6 MeV/nucleon incident energy and an impact parameter of b=5 fm. The spectra result from coupled-channels calculations using the Rutherford trajectory (thin solid lines), the trajectory predicted by the one-body dissipation model (dashed line) and the dissipative diabatic model (dashed-dotted and thick solid lines) for different values of the parameters α and β (left part: α=10; right part: β=0.1).

The dissipative diabatic case with β=0 on the left-hand side has no minimum since it corresponds to a trajectory where the two nuclei bounce off the diabatic potential without forming a stretched neck. As mentioned before, the reason is that with the choice β=0 the relaxation rate $\lambda_{\rm intr}$ is somewhat too small in the early stage of the reaction. With increasing β the minimum moves towards smaller energies and becomes more pronounced. This nicely demonstrates the influence of β on the contact time. In the measured spectra the minimum is smeared out due to fluctuations and is not as clearly visible as in Fig. 14, which is obtained from a single trajectory with the impact parameter b=5 fm. The steeper decrease of the spectrum below 2 MeV, however, is preserved and gives a measure of the atomic time $t_{\rm ato}$. It is mainly the low-energy part of the spectrum and hence the atomic time which is sensitive to the parameter β as can be seen on the left-hand side of Fig. 14. The right-hand side shows that the new dissipative diabatic model increases the high-energy yield by an order of magnitude as compared to the Markovian one-body dissipation model which is a clear evidence for fast stopping in the approach phase.

The influence of the parameters α, β, and t^* on the atomic contact time is summarized in Fig. 15. Although the atomic contact time does not allow to determine uniquely the different parameters which influence the relaxation rate, Fig. 15 shows that the values for α, β, and t^*, which have been estimated from microscopic considerations in the previous section, are within the acceptable range for reproducing the correct atomic contact time.

C. Comparison with experimental data

In Fig. 16 the measured δ-electron spectra obtained from Pb+Pb collisions at 12 MeV/nucleon, shown for four different TKEL bins, are compared with coupled-channels calculations [47]. All calculations are multiplied by the same overall factor of 1.5 to match the measured spectra at low energies. In the upper part the displayed δ-electron spectrum is measured in coincidence with elastic collisions. The spectrum calculated with the Rutherford trajectories coincides with the mea-

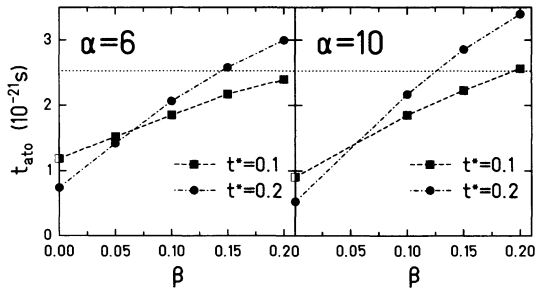

FIG. 15. Influence of the parameter α, β, and t^* (in units of 10^{-21} s) on the atomic contact time for central collisions of Pb+Pb at 8.6 MeV/nucleon incident energy (for the definition of $t_{\rm ato}$ see text). The horizontal dotted line denotes the atomic time obtained with the one-body dissipation model.

sured one. The impact-parameter distributions of all trajectories are chosen appropriate to the measured TKEL bin (Sec. III A). With increasing TKEL of the reaction the spectra become steeper than the ones calculated from Rutherford trajectories (dotted lines). This effect is due to the time delay caused by the nuclear interaction between the heavy ions. The increase in the time delay between ingoing and outgoing trajectories is reproduced by both the one-body dissipation model and the dissipative diabatic model (dashed and full lines, respectively).

But compared to previous investigations [7,9], in the present work the electron spectra are measured up to 8 MeV which improves the time resolution by a factor of 2 so that more details (not only the overall interaction time) of the dynamical evolution become visible. Remembering that according to Eq. (1) the δ-electron energies correspond to the Fourier frequencies contained in the time evolution of the rms charge radius one sees in Fig. 16 that for the highest TKEL bin (or an average impact parameter of b=9 fm) there must be rapid changes in the rms radius since the yield of δ electrons in the energy range between 6 and 8 MeV is more than a factor of 10 higher than in the lower TKEL bins. As discussed in the previous section this effect is absent in the Markovian one-body dissipation model but is explained well in the dissipative diabatic picture by the elastoplasticity of the nuclei. During the initial phase of the collision the nuclei are stopped rapidly by the diabatic potential which is built up during a short time. The diabatically stored energy is then dissipated during a damped giant vibration which in the model is mainly of quadrupole type. The energy of 7 MeV around which the δ-electron yield is enhanced corresponds to a rather low excitation energy for a giant quadrupole vibration and hence to a large mass number. If one extrapolates simply the phenomenological relation $E_{\rm osc} \approx 63$ MeV $A^{-1/3}$ for the energy of the giant quadrupole resonance of stable nuclei [48], one gets $E_{\rm osc}$ = 8.4 MeV for A=416 and $E_{\rm osc}$=10.6 MeV for A=208. Taking into account that the combined system with A=416 is rather elongated, which, compared to a spherical shape, decreases the frequency further [49], one may conjecture that one sees for the first time the giant vibration of a nuclear system with mass number A=416.

In order to show the strength of the oscillations, the nuclear trajectories are displayed in Fig. 17 for an impact parameter of b=9 fm which corresponds to the highest TKEL window. In the upper part the rms charge radius obtained in the dissipative diabatic model shows a faster stopping and a shorter interaction time than the one-body dissipation model. But the damped oscillation is much less pronounced for this impact parameter than in the head-on collisions (cf. Fig. 1 for the 12 MeV/nucleon

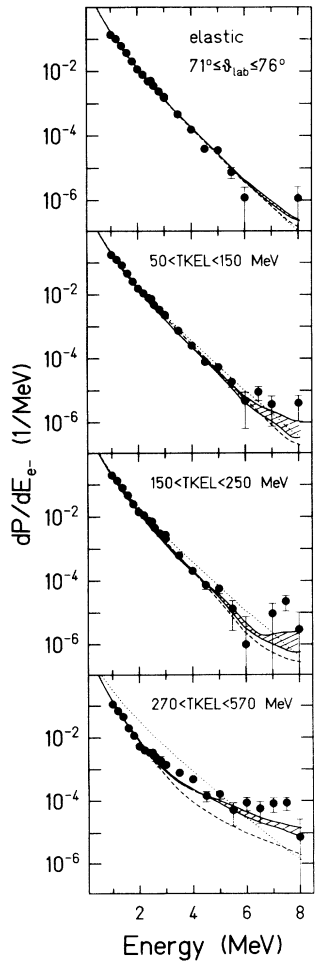

FIG. 16. Spectra of electron emission probability per collision of Pb+Pb at 12 MeV/nucleon incident energy. The curves are results of coupled-channels calculations based on the nuclear trajectories predicted by various reaction models (dotted: Rutherford trajectories; dashed: one-body dissipation model; hatched area in between the solid lines: dissipative diabatic model with α=6–12 and β=0.15).

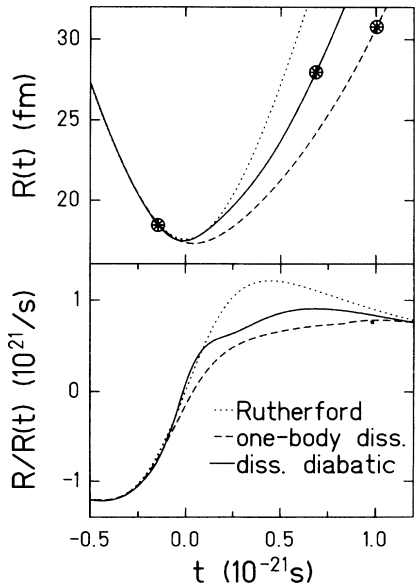

FIG. 17. Nuclear trajectories in terms of twice the root-mean-square radius $R(t)$ and $\dot{R}/R(t)$ as a function of time for b=9 fm corresponding to the highest TKEL window. The spoke-wheel symbols denote the instants of touching and separating shapes as defined in Ref. [17].

or Figs. 12 and 13 for the 8.6 MeV/nucleon case). The quantity $\dot{R}/R(t)$, to which the δ-electron yield is sensitive, is depicted in the lower part of Fig. 17. Here the elastoplastic effects which are responsible for the enhancement around 7 MeV, are seen more clearly than in $R(t)$ itself. The hatched area in between the solid lines in Fig. 16 are the theoretical predictions obtained with the elastoplastic model using β=0.15 and α values between 6 and 12. Values of α larger than 12 do not change the result significantly. At high TKEL values the intrinsic equilibration rate is mainly determined by two-body collisions, leading to a weak sensitivity on the parameter β.

Altogether one can conclude that the faster stopping predicted by the dissipative diabatic model leads to the increased yield of high-energy δ electrons, thus resulting in a much better description of the measured spectra.

It might be of interest to mention the unexpected high yield of δ electrons (up to 2.5 MeV) emitted in quasielastic heavy-ion collisions where the influence of fast changes of $\dot{R}/R(t)$ on the spectral distribution of δ electrons is discussed by assuming phenomenological trajectories [50]. Guided by these experimental results the influence of giant resonances of the two individual nuclei on the production of δ electrons in heavy-ion collisions is investigated in Ref. [51]. There it is shown that reasonable parameters for the amplitude and the frequency of the giant resonance of the individual nuclei lead to almost negligible modifications of the δ-electron spectra in the measured range up to 2.5 MeV and cannot explain the enhancement in the measured spectra.

Next it will be demonstrated that not only the δ-electron spectra are explained but also the measured kinematical correlations of the heavy ions are reproduced better with the new dissipative diabatic model. On the left-hand side of Fig. 18 the experimental correlations of the scattering angle θ_e (ejectile) and θ_p (projectile) are shown for collisions of Pb+Pb at 8.6 and 12 MeV/nucleon incident energy, while the right-hand side displays the (TKE,ϑ_e) distributions. The data correspond to deep inelastic collisions where both reaction partners survive without undergoing sequential fission. The comparison with the theoretical predictions for the position of the ridge in the double-differential cross section shows, that for both, the 8.6 and the 12 MeV/nucleon data, the dissipative diabatic model (full lines) is in better agreement with the measured distributions. The total kinetic-energy loss predicted by the one-body dissipation calculation (dashed lines) is too high which leads to the stronger focussing of the trajectories. This behavior is obviously not confirmed by the experimental data. The differences between the one-body dissipation and the dissipative diabatic model are smaller for the 12 MeV/nucleon data. The reason is that these collisions lead to a higher amount of intrinsic energy already in the beginning of the reaction and thus due to the shorter relaxation time the system reaches the dissipative limit sooner. Since the measurements represent always a time integral over the whole dynamical evolution the signatures of the shortened diabatic phase are weakened. This decreasing sensitivity is in contrast to the δ-electron spectra which give information about details of the time evolution and therefore higher beam energies are more suited to bring out the diabatic effects caused by an intrinsic relaxation which is slower than the rapid changes in the macroscopic variables.

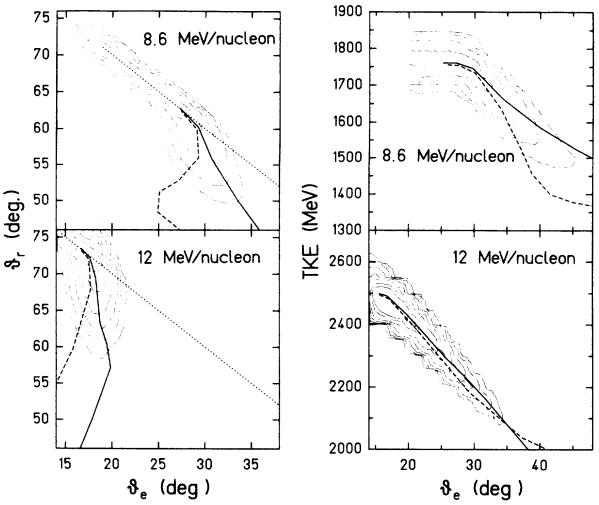

FIG. 18. Measured kinematical correlations (scattering angle of ejectile versus angle of recoil, left-hand part) and (TKE,ϑ_e) distributions (rhs) for the system Pb+Pb at 8.6 MeV/nucleon (upper part) and 12 MeV/nucleon (lower part) incident energy. The data are compared with theoretical predictions obtained with the one-body dissipation model (dashed lines) and the dissipative diabatic model with α=10 and β=0.15 (solid line). The dotted lines denote the correlations for elastic scattering.

In Fig. 19 the δ-electron spectrum measured in dissipative Pb+Pb collisions at 8.6 MeV/nucleon incident energy [9] is compared with the dissipative diabatic model calculation using the parameters $t^* = 2 \times 10^{-21}$ s, α=10, and β=0.2, which give a perfect fit. As shown in Fig. 15 in the preceding section the value of β=0.2 leads to longer atomic contact times than predicted by the one-body dissipation model. The steep decrease of the experimental data seems to indicate that in this case collisions

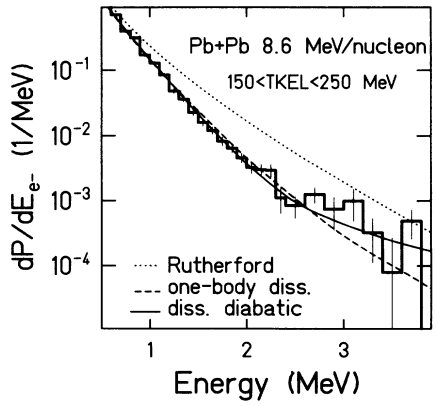

FIG. 19. δ-electron spectrum from dissipative collisions of Pb+Pb at 8.6 MeV/nucleon [9] (dotted line: Rutherford trajectory; dashed line: one-body dissipation model; solid line: dissipative diabatic model using α=10 and β=0.2).

with somewhat longer contact times contribute to the selected TKEL window. However, here the electron energies have only been measured up to 4 MeV and, hence, only the onset of the high-energy enhancement due to diabatic effects is seen.

V. DISCUSSION AND CONCLUSION

The dissipative diabatic model presented in this work allows for a consistent description of dissipative heavy-ion collisions. The good agreement of the δ-electron spectra measured in coincidence to dissipative heavy-ion collisions and the theoretical predictions obtained with the dissipative diabatic model strongly supports the existence of an elastoplastic behavior of nuclear matter in dissipative heavy-ion collisions. Especially the important requirement that both the fast deceleration and the prolonged nuclear contact time, which are reflected by the measured δ-electron spectra, should be described by the theoretical approach is met well by the new model. Within the Markovian one-body dissipation model of Ref. [17] this requirement could not be fulfilled.

The modification of the existing one-body dissipation model by replacing the Markovian friction forces with an elastoplastic force [22] should be regarded as a first attempt to describe heavy-ion collisions over the whole impact parameter regime leading to dissipative collisions without using the most questionable Markov assumption applied in all other friction models. Experimental observables expected from an elastoplastic behavior of nuclear matter have been extensively studied within this model [22]. Besides the good agreement obtained for the description of fusion-barrier heights and fluctuations [52] the results presented in this work serves as an additional support for an elastoplastic behavior of nuclear matter. The dissipative diabatic model serves as a link between time-dependent Hartree-Fock calculations and the stochastic reaction models with time-local friction forces.

However, unsatisfactory in this approach is the approximate evaluation of the stiffness tensor from Eq. (8). A consistent microscopic model could be based on the fluid-dynamical formulation of dissipative diabatic dynamics [53,54] where the stiffness tensor is directly related to the microscopic velocity field. Since this velocity field is already calculated in the one-body dissipation model [17] we are developing an improved version of the dissipative diabatic model.

Within the dissipative diabatic model a crucial parameter is the intrinsic equilibration rate which shows a great sensitivity on the theoretical predictions. In addition to the relaxation via residual two-body collisions, two additional contributions are important: the static and the acceleration coupling between diabatic single-particle states. These have been estimated theoretically. The systems examined experimentally in this paper do not allow for a unique determination of the individual strength of the several contributions to the relaxation processes.

In addition to the good agreement of the theoretical and the experimental δ-electron spectra for Pb+Pb collisions at 8.6 and 12 MeV/nucleon the comparison of the (TKE,ϑ) distributions further supports the dissipative diabatic approach. The tendency of the trajectories to focus for energy losses around 250 MeV, as predicted by the one-body-dissipation model, is not confirmed by the experimental distributions. A much better description is obtained with the dissipative diabatic model.

The careful analysis of the δ-electron spectra and the (TKE,ϑ) distributions of the Pb+Pb reactions at 8.6 and 12 MeV/nucleon indicates that nuclear matter is elastoplastic as predicted by the diabatic approach to dissipative collective motion [22].

ACKNOWLEDGMENTS

We would like to thank S. Graf and Th. de Reus from the University of Frankfurt for their help in running the coupled-channels code. The construction of dedicated electronic units by J. Foh and the electronic workshop and the production of the large-area silicon counter by W. Patzner both of the Institut für Kernphysik, Darmstadt as well as the preparations of the targets by H. Folger and the GSI target laboratory is gratefully acknowledged. This work is supported by the Bundesministerium für Forschung und Technologie under Contract No. 06DA453 and by the Gesellschaft für Schwerionenforschung, Darmstadt.

[1] H. Nifenecker and J. A. Pinston, in *Progress in Particle and Nuclear Physics*, edited by A. Faessler (Pergamon, New York, 1990), Vol. 23; V. Metag, Ann. Phys. **48**, 121 (1991).
[2] W. Nörenberg, Nucl. Phys. **A482**, 221c (1988).
[3] G. Soff, J. Reinhardt, B. Müller, and W. Greiner, Phys. Rev. Lett. **43**, 1981 (1979).
[4] E. Kankeleit, Nukleonika **25**, 253 (1980).
[5] H. Backe, P. Senger, W. Bonin, E. Kankeleit, M. Krämer, R. Krieg, V. Metag, N. Trautmann, and J. Wilhelmy, Phys. Rev. Lett. **50**, 1838 (1983).
[6] R. Kreig, E. Bożek, U. Gollerthan, E. Kankeleit, G. Klotz-Engmann, M. Krämer, U. Meyer, H. Oeschler, and P. Senger, Phys. Rev. C **34**, 562 (1986).
[7] M. Krämer, B. Blank, E. Bożek, E. Kankeleit, G. Klotz-Engmann, C. Müntz, H. Oeschler, and M. Rhein, Phys. Lett. B **201**, 215 (1988).
[8] J. Stroth, H. Backe, M. Begemann-Blaich, H. Bokemeyer, P. Glässel, D. v. Harrach, W. Konen, P. Kosmadakis, S. Mojumder, P. Senger, and K. Stiebing, in *Proceedings of the XXVI International Winter Meeting on Nuclear Physics*, Bormio, 1988, edited by I. Iori (Ric. Sci. Educ. Permanente Bormio, 1988).
[9] M. Krämer, B. Blank, E. Bożek, E. Kankeleit, G. Klotz-Engmann, C. Müntz, H. Oeschler, M. Rhein, and P. Senger, Phys. Rev. C **40**, 1662 (1989).
[10] U. Müller, G. Soff, J. Reinhardt, T. de Reus, B. Müller, and W. Greiner, Phys. Rev. C **30**, 1199 (1984).

[11] E. Kankeleit, in *International Advanced Courses on "Physics of Strong Fields,"* edited by W. Greiner (Plenum, New York, 1987).
[12] W. U. Schröder and J. R. Huizenga, in *Treatise on Heavy-Ion Science*, edited by D. A. Bromley (Plenum, New York, 1984), Vol. 2, and references therein.
[13] R. Bass, *Nuclear Reactions with Heavy Ions* (Springer-Verlag, Berlin, 1980).
[14] W. Nörenberg and H. A. Weidenmüller, *Introduction to the Theory of Heavy-Ion Collisions* (Springer-Verlag, Berlin, 1980).
[15] P. Fröbrich and J. Stroth, Phys. Rev. Lett. **64**, 629 (1990).
[16] R. Schmidt, V. D. Toneev, and G. Wolschin, Nucl. Phys. **A311**, 247 (1978).
[17] H. Feldmeier, Rep. Progr. Phys. **50**, 915 (1987).
[18] Th. de Reus, J. Reinhardt, B. Müller, U. Müller, G. Soff, and W. Greiner, Z. Phys. A **321**, 589 (1985).
[19] M. D. Rhein, Ph.D. thesis, Institut für Kernphysik, Technische Hochschule Darmstadt, 1991; GSI Scientific Report No. GSI-92-20, 1992.
[20] M. Rhein, R. Barth, E. Ditzel, H. Feldmeier, E. Kankeleit, V. Lips, C. Müntz, W. Nörenberg, H. Oeschler, A. Piechaczek, W. Polai, and I. Schall, Phys. Rev. Lett. **69**, 1340 (1992).
[21] J. Blocki, Y. Boneh, J. R. Nix, J. Randrup, M. Robel, A. J. Sierk, and W. J. Swiatecki, Ann. Phys. (N.Y.) **113**, 330 (1978).
[22] W. Nörenberg, Phys. Lett. B **104**, 107 (1981); W. Nörenberg, in *Heavy Ion Reaction Theory*, edited by W. Q. Shen, J. Y. Li, and L. X. Ge (World Scientific, Singapore, 1989); in *New Vistas in Nuclear Dynamics*, edited by P. J. Brussard and J. H. Koch (Plenum, New York, 1986).
[23] E. Kankeleit, U. Gollerthan, G. Klotz, M. Kollatz, M. Krämer, R. Krieg, U. Meyer, H. Oeschler, and P. Senger, Nucl. Instrum. Methods A **234**, 81 (1985).
[24] M. Rhein and Ch. Müntz, GSI Scientific Report No. GSI-89-01, 1989.
[25] I. Schall, E. Kankeleit, H. Oeschler, and M. D. Rhein, GSI Scientific Report No. GSI-89-01, 1989.
[26] L. Pages, E. Bertels, H. Joffre, and L. Sklaventitis, At. Data **4**, 2 (1972).
[27] W. Polai, Diploma thesis, Institut für Kernphysik, TH-Darmstadt, 1992.
[28] H. J. Wollersheim, W. W. Wilke, J. R. Birkelund, and J. R. Huizenga, Phys. Rev. C **25**, 338 (1982).
[29] P. Glässel, D. v. Harrach, H. J. Specht, and L. Grodzins, Z. Phys. A **310**, 189 (1983).
[30] N. Diamond, Nukleonika **21**, 29 (1976).
[31] R. J. Liotta, Nucl. Phys. **A297**, 136 (1978).
[32] C. Kozhuharov, P. Kienle, E. Berdermann, H. Bokemeyer, J. S. Greenberg, Y. Nakayama, P. Vincent, H. Backe, L. Handschug, and E. Kankeleit, Phys. Rev. Lett. **42**, 376 (1979).
[33] H. Backe, W. Bonin, E. Kankeleit, M. Krämer, R. Krieg, V. Metag, P. Senger, N. Trautmann, F. Weik, and J. Wilhelmy, in *QED of Strong Fields*, Vol. 80 of *NATO Advanced Study Institute Series B*, edited by W. Greiner (Plenum, New York, 1983), p. 107.
[34] M. Krämer, B. Blank, E. Bożek, E. Ditzel, E. Kankeleit, G. Klotz-Engmann, C. Müntz, H. Oeschler, and M. Rhein, Phys. Lett. B **245**, 17 (1990).
[35] H. Tsertos, E. Berdermann, F. Bosch, M. Clemente, S. Huchler, P. Kienle, W. König, and C. Kozhuharov, Z. Phys. A **342**, 79 (1992), and references therein.
[36] P. Schlüter, G. Soff, and W. Greiner, Phys. Rep. **75**, 327 (1981).
[37] R. S. Hager, E. C. Seltzer, and V. F. Trusov, in *Atomic and Nuclear Data Reprints, Internal Conversion Coefficients*, edited by K. Way (Academic, New York, 1973).
[38] M. Rhein, R. Barth, E. Ditzel, E. Kankeleit, V. Lips, C. Müntz, H. Oeschler, A. Piechaczek, W. Polai, and I. Schall (unpublished).
[39] J. Randrup, Nucl. Phys. A **327**, 490 (1979).
[40] G. F. Bertsch, Z. Phys. A **289**, 103 (1987).
[41] W. Cassing and W. Nörenberg, Nucl. Phys. **A433**, 467 (1985).
[42] A. Lukasiak, W. Cassing, and W. Nörenberg, Nucl. Phys. **A426**, 181 (1984).
[43] W. J. Swiatecki and S. Björnholm, Phys. Rep. **4**, 247 (1972).
[44] W. U. Schröder and J. R. Huizenga, Ann. Rev. Nucl. Sci. **27**, 465 (1977).
[45] P. Rozmej and W. Nörenberg, Phys. Lett. B **117**, 278 (1986).
[46] J. Reinhardt, B. Müller, and W. Greiner, Z. Phys. A **292**, 211 (1979).
[47] Th. de Reus, U. Müller-Nehler, G. Soff, J. Reinhardt, S. Graf, B. Müller, and W. Greiner, Phys. Rev. C **40**, 752 (1989).
[48] H. Sagawa and G. Holzwarth, Progr. Theor. Phys. **59**, 1213 (1979).
[49] A. Lukasiak and W. Nörenberg, Z. Phys. A **326**, 79 (1987).
[50] S. Mojumder, Ph.D. thesis, Universität Frankfurt 1990, Report GSI-90-12 (1990); J. Stroth, Ph.D. thesis, Universität Mainz 1990, Report GSI-90-28 (1990).
[51] S. Graf, D. Troltenier, A. Schäfer, and W. Greiner, Z. Phys. A **343**, 209 (1992).
[52] D. Berdichevsky, A. Lukasiak, W. Nörenberg, and P. Rozmej, Nucl. Phys. **A499**, 609 (1989); **A502**, 395c (1989).
[53] B. Morgenstern and W. Nörenberg, Nucl. Phys. **A492**, 93 (1989).
[54] C. E. Vignolo, W. Nörenberg, E. S. Hernandez, and S. Ayik (unpublished).

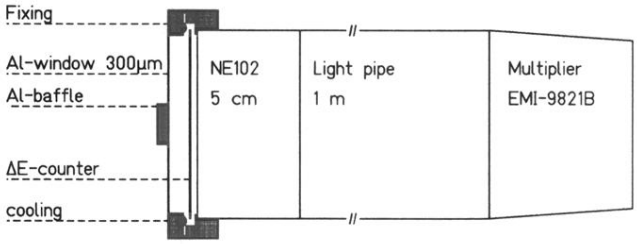

FIG. 3. Components of the plastic detector designed to measure electrons in the energy range of 2 MeV up to 8 MeV.